Optics Letters

Generation of a vector light field based on polarization holography

Lu Huang,[1] Yuanying Zhang,[1,2] Qi Zhang,[1] Yuxin Chen,[1] Xi Chen,[1] Zhiyun Huang,[1] Xiao Lin,[1] and Xiaodi Tan[1,3]

[1]College of Photonic and Electronic Engineering, Key Laboratory of OptoElectronic Science and Technology for Medicine of Ministry of Education, Fujian Provincial Key Laboratory of Photonics Technology, Fujian Normal University, Fuzhou 350117, China
[2]e-mail: zhangyy@fjnu.edu.cn
[3]e-mail: xtan@fjnu.edu.cn

Received 19 July 2021; revised 13 August 2021; accepted 15 August 2021; posted 16 August 2021 (Doc. ID 438070); published 9 September 2021

We propose a simple and effective method for generating a vector light field based on the faithful reconstruction (FR) effect of polarization holography, where the arbitrary linear polarization waves can be faithfully reconstructed by the polarization-sensitive recording media. The scheme incorporates the tunable and switchable dynamics exposure system to manufacture vector beams. By regulating the velocity and the initial polarization through the angle-aperture and the half-wave plate in the dynamics exposure system, the generated optical element can convert a linear polarization wave into a vector beam. We have analyzed the feasibility in theory and demonstrated the generation of the vector beams experimentally which shows good agreement with the theoretical simulations.

https://doi.org/10.1364/OL.438070

Distinguished from the traditional scalar light field with isotropic polarization distribution, the vector light field refers to the light field with anisotropic polarization states at different positions on the same wavefront simultaneously. Among the categories of the vector beam, the radial beam exhibits an excellent ability to focus the plane wave in the subwavelength regime [1]. Until now, the vector light field has been widely desirable for various applications, including optical trapping [2], optical and quantum communications [3], quantum memories [4], laser manufacturing [5], and nonlinear optics [6] for its unique characteristics [7]. Thus, the generation of the vector light field is one of the research hotspots. At present, a large number of methods for generating the vector light fields have been proposed. In general, the approaches can be classified into two mainstreams. One is achieved by the optical element such as the photo-controlled orientated liquid crystal [8], subwavelength grating [9], and metamaterial [10]. Another is by the assistance of the optical instrument such as a spatial light modulator (SLM) [11] or spiral phase plate [12] which produces orthogonal components of the vector beam, and then superimposes them coaxially into the vector light field by the interferometry.

In this Letter, we propose a new strategy to generate vector light fields based on the polarization holography. Polarization holography, which not only records the amplitude and phase information of the light field as traditional holography, but also can faithfully record and reconstruct the polarization information of the light field [13]. Recently, the polarization holography was also applied in generating the vector light fields with spatially variant amplitude, phase, and polarization by means of two polarization holograms [14]. However, research has been limited to the paraxial approximation, which will more or less confine the flexibility of designing the polarization interference field, until Kuroda [15] proposed a new tensor theory to describe the interference between different polarization waves which breaks through the paraxial limitation. Since then, various interesting polarization holography properties have been reported such as the null reconstruction effect [16] and the faithful reconstruction (FR) effect. Among these characteristics, the FR is one of the most significant phenomena, which means that the reconstructed wave is identical to the signal wave, indicating that the intensity, phase, and polarization state of the information can be recorded and reconstructed simultaneously [17]. The investigations refer to the FR of linear [17–19], circular [20] and orthogonal elliptical polarization [21], which have the potential applications in high-density optical data storage [22,23], the circular polarization wave generator, [24] and so on.

Using the tensor theory proposed by Kuroda [15], we present a schematic diagram to prepare the vector light fields, which combines the advantages of the FR effect in polarization holography and the photo-induced anisotropic polymer materials. Unlike the previously reported approaches, our proposed method is supported by a concise and dynamic tunable exposure system which not only gets rid of all the auxiliary elements such as SLM [25] and Q-plate [26], but also has the advantages of being easy to fabricate and saving time. By setting the initial polarization and regulating the relative rotation speed in the dynamics exposure system, variant vector beams can be generated directly in a flexible way.

Here we use a schematic diagram to characterize the mechanism of the tensor theory in polarization holography, as shown

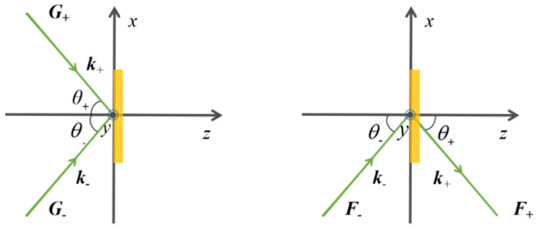

Fig. 1. Schematic diagram of polarization holography. (a) Recording stage and (b) reconstruction stage.

in Fig. 1. The beams in the recording and reconstructing process are denoted by $\boldsymbol{G}$ and $\boldsymbol{F}$.

The $\boldsymbol{p}$-polarized is defined as the beam polarized in the x-z plane, which is perpendicular to the wave propagation; the $\boldsymbol{s}$-polarized is parallel to y axis, and $\boldsymbol{k}$ is the wave vector which can be denoted as follows:

$$\boldsymbol{s} = \begin{bmatrix} 0 \\ 1 \\ 0 \end{bmatrix}, \quad \boldsymbol{p}_j = \begin{bmatrix} \cos\theta_j \\ 0 \\ \sin\theta_j \end{bmatrix}, \quad \boldsymbol{k}_i = \begin{bmatrix} k\sin\theta_i \\ 0 \\ k\cos\theta_i \end{bmatrix}, \tag{1}$$

where $j(+,-)$, $i(+,-)$. The subscription "+" and "−" are applied to distinguish the component of signal and reference waves, respectively. The two beams interfere at a symmetrical angle of $\theta_+ = \theta_-$, and the resultant electric field can be represented by

$$\boldsymbol{E} = \boldsymbol{G}_+ e^{i\boldsymbol{k}_+\cdot\boldsymbol{u}} + \boldsymbol{G}_- e^{i\boldsymbol{k}_-\cdot\boldsymbol{u}}, \tag{2}$$

where $\boldsymbol{u}$ is position vector.

Here in our scheme, in the recording stage, the arbitrary linear polarization waves are employed as the signal wave which can be written as

$$\boldsymbol{G}_+ \propto (\alpha\boldsymbol{s} + \beta\boldsymbol{p}_+), \tag{3}$$

where α and β are coefficients of arbitrary real numbers. For reconstructing the arbitrary linear polarization waves $\boldsymbol{G}_+$, the interference field should be designed to satisfy the FR condition such that $\boldsymbol{p}$-polarized wave is adopted as the reference wave $\boldsymbol{G}_-$.

In the reconstruction stage, with reading wave of the $\boldsymbol{p}$-polarized state, the reconstructed wave can be expressed as

$$\boldsymbol{F}_+ \propto B(\alpha s + \beta p_+) + (A+B)\beta\cos^2\theta\boldsymbol{s}, \tag{4}$$

where A and B represent the coefficients of the photo-induced isotropic and anisotropic refractive index change [15], respectively.

It can be deduced from Eq. (4) that when the interference angle is $\pi/2$, the reconstructed wave can be simplified as

$$\boldsymbol{F}_+ \propto B(\alpha s + \beta\boldsymbol{p}_+), \tag{5}$$

which is consistent with the signal wave $\boldsymbol{G}_+$. We have summarized the cases in Table 1.

Assuming the Bragg condition is satisfied, from the last column of Table 1, it can be seen that when the interference angle is $\pi/2$, the arbitrary polarization state can be faithfully reconstructed. The results indicate that the arbitrary polarization wave can be written in volume polarization grating with a well-designed interference field. Thus, the generation of vector light fields can be realized.

Table 1. FR for the Arbitrary Linear Polarization Wave

Recording		Reading	Reconstruction	
$\boldsymbol{G}_-$	$\boldsymbol{G}_+$	$\boldsymbol{F}_-$	$\boldsymbol{F}_+$	$\boldsymbol{F}_+(\theta=\pi/2)$
$\boldsymbol{p}_-$	$\alpha\boldsymbol{s}+\beta\boldsymbol{p}_+$	$\boldsymbol{p}_-$	$B(\alpha\boldsymbol{s}+\beta\boldsymbol{p}_+)+(A+B)\beta\cos^2\theta\boldsymbol{s}$	$B(\alpha\boldsymbol{s}+\beta\boldsymbol{p}_+)$

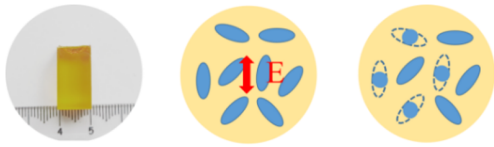

Fig. 2. Polarization-sensitive polymer material in our experiment. (a) Cubic material and (b) the molecular distribution model before exposure; E, electric vector of the light field. (c) Molecular distribution model after exposure.

In our experiments, we apply the homemade cubic phenanthrenequinone-doped polymethyl methacrylate photopolymer (PQ/PMMA) [27] with a size of approximately 10 mm × 10 mm × 30 mm, as shown in Fig. 2(a). The material is made up of anisotropic rod-shaped molecules that are randomly distributed in all directions before exposure, as shown in Fig. 2(b), so the material as a whole is isotropic from a macroscopic perspective. Under the illumination of the polarization electric wave, the rod-shaped molecules will react from anisotropic rod-shaped molecules to globular isotropic molecules due to the photo-induced effect [28], as shown in Fig. 2(c).

We utilize a Mach–Zehnder interferometer making two beams incident perpendicularly into the cubic PQ/PMMA from both sides, as shown in Fig. 3. We employ a laser with the wavelength of 532 nm, which is suitable for the polymer material. The beam is divided by a polarization beam splitter (PBS) into two paths for recording and reconstructing the signal wave. In the recording stage, the reference wave and signal wave are separated with the intensity ratio of 2:1, where the $\boldsymbol{p}$-polarized beam transmitted from the PBS serves as the reference wave (1 mW). Likewise, the beam reflected from the PBS is utilized as a signal wave which is modulated by a half-wave plate (HWP) and a dynamically adjustable angle-aperture which can regulate the exposure areas and dosage. Then L1 and L2 with a focal length of 75 mm constitute a 4-f system that can image the angle-aperture image on the recording material. In the reconstruction stage, the reconstruction wave is $\boldsymbol{p}$-polarized. L3 with a focal length of 100 mm is applied to image the generated vector light field on a CMOS. A polarizer (P3) is employed before the CMOS for characterizing the polarization properties of the vector beams.

In the signal wave path, the dynamics exposure system constitutes a HWP and a specially designed angle-aperture (0.2°), which is stacked by two angle-apertures sheets, as shown in Fig. 4(a). The angle-aperture and the HWP are installed separately in the mechanical rotary device (SIGMA, GSC-02), ensuring that the rotation velocity of the HWP and the angle-aperture can be modulated independently. Thus, the relative rotation speed between the HWP and the angle-aperture can be adjusted directly in a flexible way.

In general, the polarization state of the vector beams can be represented as [29]

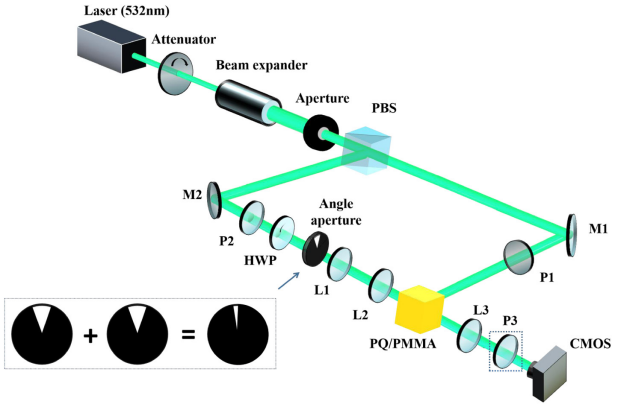

Fig. 3. Experimental setup. PBS, polarization beam splitter; HWP, half-wave plate; M, mirror; P, polarizer; L, lens; CMOS, complementary metal oxide semiconductor.

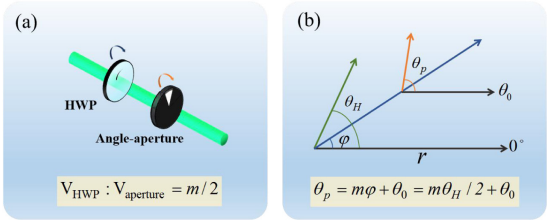

Fig. 4. Principle of generating vector light fields; (r, φ) is the polar coordinates representation. (a) Schematic diagram of the dynamical exposure system consisting of the angle-aperture and the HWP; V_{aperture} and V_{HWP} correspond to the rotation velocity of the angle-aperture and the HWP. (b) Polarization relations between the HWP and the resultant polarization θ_p in the polar coordinates.

$$\theta_p = m\varphi + \theta_0, \tag{6}$$

where θ_p is the resultant polarization state, and θ_0 is a constant describing the initial polarization state at $\varphi = 0$ azimuthally. m can be an integer or semi-integer denoting the azimuthal index of the vector light field.

The Jones matrix of the HWP can be described as follows:

$$J_{\lambda/2} = \begin{bmatrix} \cos 2\varphi & \sin 2\varphi \\ \sin 2\varphi & -\cos 2\varphi \end{bmatrix}, \tag{7}$$

when s-polarized passes through the HWP with its fast axis at the position of φ, θ_H is the polarization direction after the HWP, and the resultant Jones vector can be described as

$$J_{\text{out}} = \begin{bmatrix} \cos 2\varphi & \sin 2\varphi \\ \sin 2\varphi & -\cos 2\varphi \end{bmatrix} \begin{bmatrix} 0 \\ 1 \end{bmatrix} = \begin{bmatrix} \sin 2\varphi \\ -\cos 2\varphi \end{bmatrix} = \begin{bmatrix} \sin\theta_H \\ -\cos\theta_H \end{bmatrix}. \tag{8}$$

According to Eq. (8), it can be derived that the $\theta_H = 2\varphi$. Therefore, the azimuthal angle φ in Eq. (6) can be represented by θ_H; then the vector beam generated in our system can be transformed into

$$\theta_p = m\theta_H/2 + \theta_0, \tag{9}$$

where θ_p is the resultant polarization direction after the exposure system. For the vector beam with the azimuthal index of m, the relative velocity ratio between the angle-aperture and the HWP is $m/2$.

The angular dependence between the resultant linear polarization state and the rotation angle of the HWP can be illustrated in Fig. 4(b) [30]. The blue arrow represents the relative azimuthal angle φ of the HWP with respect to the horizontal direction. The green arrow θ_H represents the polarization direction after the HWP. While setting the initial polarization state θ_0, the vector beam of the local linear state of polarization will append an azimuthal variation in the polarization direction which will produce the resultant polarization direction θ_p denoted by the orange arrow, such that, by delicately modulating the initial polarization state θ_0, and the relative velocity between the HWP and the angle-aperture, variant vector beams can be obtained by the proposed experimental scheme.

To verify our proposed method, we generate the vector beams with the azimuthal index of $m = 1, 2$. Without loss of generality, we also produce the vector beams with different initial polarization θ_0.

Figures 5(a) and 6(a) show the simulation intensity corresponding to the vector beams with the azimuthal index of $m = 1$ and the initial polarization state of $\theta_0 = 0°$ and $\theta_0 = 15°$, respectively.

In order to generate variant vector beams, the relative rotational speed of the HWP and the angle-aperture are adjusted according to the azimuthal index m, as indicated in Eq. (9). Here, for the case of $m = 1$, the relative speed of the angle-aperture is twice as fast as the HWP, with a rotating speed of 1°/s and 0.5°/s, respectively. At the start of the exposure process, both the fast axis of the HWP and the gap of the angle-aperture are situated at the positive horizontal direction. Moreover, the case of $\theta_0 = 15°$ means that the wave has a polarization angle of 15°, referring to the horizontal direction at the azimuthal angle of $\varphi = 0$, such that, by regulating the fast axis of the HWP to be 0° or 7.5° with respect to the horizontal direction, the desired initial θ_0 of the vector beam will spontaneously modulated to be $\theta_0 = 0°$ or $\theta_0 = 15°$. The intensity and polarization distributions are shown in Figs. 5 and 6, where the first and second rows are the corresponding simulation and experimental results.

Simulations of the polarization maps of the vector beams are shown in Figs. 5(b)–5(e) and 6(b)–6(e). The observed patterns are split into two lobes. Figures 5(g)–5(j) and 6(g)–6(j) are the corresponding experimental results; we notice that the generated vector beams are in accord with the simulation results.

In addition, to better reveal the flexibility of our proposed scheme, the vector beam with the azimuthal index of $m = 2$ is also generated.

According to Eq. (9), the azimuthal index of m is obtained by adjusting the HWP and the angle-aperture, satisfying the

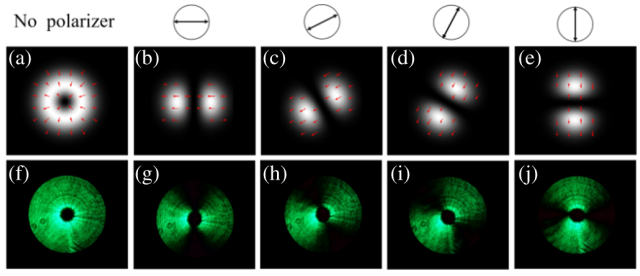

Fig. 5. Intensity and polarization distributions of the vector beam with an azimuthal index of $m = 1$, $\theta_0 = 0°$. (a), (f) Simulation and experimental intensity distributions, respectively; (b)–(e) intensity distributions after the polarizer at P = 0°, 30°, 60°, and 90° in simulation; (g)–(j) corresponding experimental results.

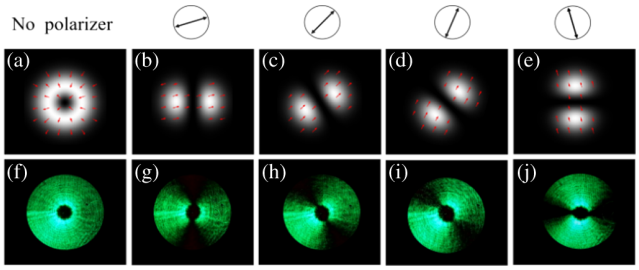

Fig. 6. Intensity and polarization distributions of the vector beam with an azimuthal index of $m = 1$, $\theta_0 = 15°$. (a), (f) Simulation and experimental intensity distributions, respectively; (b)–(e) intensity distributions after the polarizer at P = 15°, 45°, 75°, and 105° in simulation; (g)–(j) corresponding experimental results.

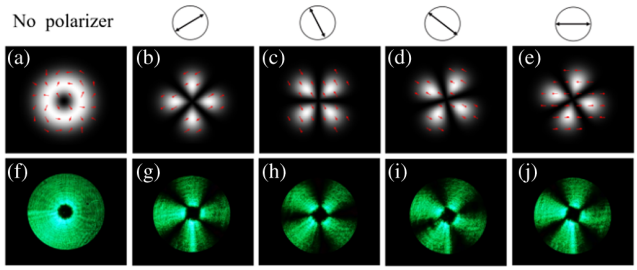

Fig. 7. Intensity and polarization distributions of the vector beam with an azimuthal index of $m = 2$ and $\theta_0 = 30°$. (a), (f) Simulation and experimental intensity distributions, respectively; (b)–(e) intensity distributions after the polarizer at P = 30°, 120°, 150°, and 180° in simulation; (g)–(j) corresponding experimental results.

rotation ratio condition of $m/2$. For the case of $m = 2$ and $\theta_0 = 30°$, $m = 2$ can be achieved by setting the angle-aperture and the HWP rotated at the same speed. Then the desired initial polarization $\theta_0 = 30°$ of the vector beam is realized by regulating the fast axis of the HWP to be 15° referring to the horizontal direction. The simulation and experimental intensity distributions are shown in Fig. 7. The analyzed intensity patterns are observed to split into four lobes, showing more complicated polarization distribution. Due to the high sensitivity of the photo-induced materials, a slight over-exposure will result in a local enhancement of the vector beams. Obviously, for the cases of $m = 1$ and $m = 2$, the obtained experimental results are consistent with the theoretical simulations, which validates that our dynamical exposure system can successfully generate variant vector beams.

In conclusion, we have proposed a new method to generate vector light fields based on the FR effect of polarization holography. By setting the desired initial θ_0 and then modulating the relative rotation speed between the HWP and the angle-aperture in the dynamic exposure system, variant vector beams can be achieved directly in a flexible way. Furthermore, vector beams with an azimuthal index of $m = 1$ and $m = 2$ are investigated in simulations and experiments, which agree well with each other. Our scheme for realizing the vector light field serves as a complementary method for the existing ways, and exhibits a new possibility to manipulate the light field based on the polarization holography.

Funding. National Key Research and Development Program of China (2018YFA0701800); National Natural Science Foundation of China (NSFC) (12104091); The Special Funds of the Central Government Guiding Local Science and Technology Development (2020L3008).

Disclosures. The authors declare no conflicts of interest.

Data Availability. Data underlying the results presented in this paper are not publicly available at this time but may be obtained from the authors upon reasonable request.

REFERENCES

1. Q. Zhan, Adv. Opt. Photonics **1**, 1 (2009).
2. B. Gu, D. Xu, G. Rui, M. Lian, Y. Cui, and Q. Zhan, Appl. Opt. **54**, 8123 (2015).
3. B. Ndagano, B. Perez-Garcia, F. S. Roux, M. McLaren, C. Rosales-Guzman, Y. Zhang, O. Mouane, R. I. Hernandez-Aranda, T. Konrad, and A. Forbes, Nat. Phys. **13**, 397 (2017).
4. M. Neugebauer, P. Woźniak, A. Bag, G. Leuchs, and P. Banzer, Nat. Commun. **7**, 11286 (2016).
5. M. Meier, V. Romano, and T. Feurer, Appl. Phys. A **86**, 329 (2007).
6. L. Zhang, X. Qiu, F. Li, H. Liu, X. Chen, and L. Chen, Opt. Express **26**, 11678 (2018).
7. C. Rosales-Guzmán, B. Ndagano, and A. Forbes, J. Opt. **20**, 123001 (2018).
8. Y.-Y. Tzeng, S.-W. Ke, C.-L. Ting, A. Y.-G. Fuh, and T.-H. Lin, Opt. Express **16**, 3768 (2008).
9. A. Niv, G. Biener, V. Kleiner, and E. Hasman, Opt. Lett. **29**, 238 (2004).
10. Y. Liu, X. Ling, X. Yi, X. Zhou, H. Luo, and S. Wen, Appl. Phys. Lett. **104**, 191110 (2014).
11. X.-L. Wang, J. Ding, W.-J. Ni, C.-S. Guo, and H.-T. Wang, Opt. Lett. **32**, 3549 (2007).
12. Z. Liu, Y. Liu, Y. Ke, Y. Liu, W. Shu, H. Luo, and S. Wen, Photonics Res. **5**, 15 (2017).
13. S. Kakichashvili, Sov. J. Quantum Electron. **4**, 795 (1974).
14. U. Ruiz-Corona, P. Pagliusi, C. Provenzano, and G. Cipparrone, Appl. Phys. Lett. **102**, 161104 (2013).
15. K. Kuroda, Y. Matsuhashi, R. Fujimura, and T. Shimura, Opt. Rev. **18**, 374 (2011).
16. A. Wu, G. Kang, J. Zang, Y. Liu, X. Tan, T. Shimura, and K. Kuroda, Opt. Express **23**, 8880 (2015).
17. Z. Huang, Y. Chen, H. Song, and X. Tan, Opt. Lett. **45**, 6282 (2020).
18. P. Qi, J. Wang, H. Song, Y. Chen, L. Zhu, and X. Tan, Acta Opt. Sinica **40**, 2309001 (2020).
19. J. Wang, P. Qi, Y. Chen, A. Lin, Z. Huang, J. Hao, X. Lin, L. Zhu, and X. Tan, Opt. Express **29**, 14033 (2021).
20. Y. Hong, G. Kang, J. Zang, F. Fan, Y. Liu, X. Tan, T. Shimura, and K. Kuroda, Appl. Opt. **56**, 10024 (2017).
21. Z. Huang, C. Wu, Y. Chen, X. Lin, and X. Tan, Opt. Express **28**, 23679 (2020).
22. X. Lin, J. Liu, J. Hao, K. Wang, Y. Zhang, H. Li, H. Horimai, and X. Tan, Opto-Electron. Adv. **03**, 190004 (2020).
23. H. Horimai, X. Tan, and J. Li, Appl. Opt. **44**, 2575 (2005).
24. X. Xu, Y. Zhang, H. Song, X. Lin, Z. Huang, K. Kuroda, and X. Tan, Opt. Express **29**, 2613 (2021).
25. S. Liu, Q. Shuxia, Y. Zhang, L. Peng, D. Wu, H. Lei, and J. Zhao, Photonics Res. **6**, 228 (2018).
26. S. Slussarenko, A. Murauski, T. Du, V. Chigrinov, L. Marrucci, and E. Santamato, Opt. Express **19**, 4085 (2011).
27. J. Zang, G. Kang, P. Li, Y. Liu, F. Fan, Y. Hong, Y. Huang, X. Tan, A. Wu, T. Shimura, and K. Kuroda, Opt. Lett. **42**, 1377 (2017).
28. Y. Zhai, L. Cao, Y. Liu, and X. Tan, Materials **13**, 5562 (2020).
29. M. Stalder and M. Schadt, Opt. Lett. **21**, 1948 (1996).
30. F. Fan, T. Du, A. K. Srivastava, W. Lu, V. Chigrinov, and H. S. Kwok, Opt. Express **20**, 23036 (2012).